On a small-scale roughness of the core–mantle boundary

C. Narteau[a], J.L. Le Mouël[b], J.P. Poirier[b],*, E. Sepúlveda[b], M. Shnirman[c]

[a] *Seismological Laboratory, California Institute of Technology, Pasadena, CA, USA*
[b] *Institut de Physique du Globe de Paris, 4 place Jussieu, 75252 Paris Cedex 05, France*
[c] *International Institute of Earthquake Prediction Theory and Mathematical Geophysics, Warshavskoye shosse, 79, korp 2, Moscow 113556, Russia*

Abstract

The roughness of the core–mantle boundary, on the scale of centimeters to tens of meters, is modelled using a cellular automata method. Square cells, of the size of grains of the mantle material, on a 2-D grid, can be in one of three states corresponding to mantle silicate or oxide, core fluid saturated in light element and unsaturated core fluid. The dynamical process of evolution is defined as a stationary stochastic process without memory. Transitions of doublets of cells from one state to another are governed by parameters representing the rates of physical processes: dissolution and crystallization at the CMB and diffusion of the light element in the core fluid. With reasonable values of the parameters, the boundary roughens on the scale of grains, and a boundary layer of saturated fluid, of a few tens of centimeters thick, soon appears at the interface. An undulation with dominant wavelength of the order of a few tens of meters eventually appears. An interaction of the roughness of the CMB with the fluid flow in the core is considered as possible.   © 2001 Elsevier Science B.V. All rights reserved.

Keywords: core–mantle boundary; roughness

1. Introduction

There is a striking contrast in physical and chemical properties between the mantle and the core. The mantle is rocky, composed mostly of crystalline silicate perovskite and magnesiowüstite, with a density of 5600 kg m^{-3} near the core–mantle boundary (CMB), while the core consists of a dense ($\approx 10\,000$ kg m^{-3}) molten iron alloy with low viscosity [1].

The CMB is therefore expected to be the seat of physical–chemical interactions between core and mantle [2]. The hot liquid core can corrode the overlying mantle, preferentially dissolving the silicates and oxides along the grain boundaries and infiltrating upward into the mantle by capillarity [3,4].

The thickness of the infiltrated layer cannot exceed a few meters, corresponding to the height for which the weight of the intergranular thin sheets of dense liquid is equilibrated by the interfacial tension between crystals and molten iron [2].

On that scale, the grains of the crystalline mantle surrounded by liquid can be loosened, float at the top of the core, and go on dissolving in the

---

* Corresponding author. Tel.: +33-1-44-27-38-10;
Fax: +33-1-44-27-24-87.
E-mail address: poirier@ipgp.jussieu.fr (J.P. Poirier).

core fluid undersaturated in the light elements constitutive of mantle minerals (mostly oxygen and silicon). The core fluid is consequently enriched in these light elements, and may become saturated. However, the light elements may diffuse from the saturated toward the still unsaturated fluid. The saturated alloy enriched in elements lighter than the bulk of the core fluid is buoyant and tends to float upward near the CMB.

Two competing processes take place at the CMB: crystals of the mantle are loosened and dissolved in the fluid, while crystalline matter is redeposited at other places. The small-scale roughness of the CMB is therefore due to the dynamic equilibrium between dissolution and redeposition. This can be compared to what happens on the atomic scale in the case of a crystal surface in equilibrium with a saturated solution or saturating vapor: atoms are continually dissolved (evaporated) and deposited (condensed) on the surface, imparting to it a roughness on the atomic scale.

Thus the CMB does not move upward or downward but may acquire a roughness on scales larger than the grain size of the mantle material, superimposed to the topography at the scale of hundreds to thousand kilometers, due to mantle convection.

2. The model

Modelling of a physical system necessarily involves the use of simplifying assumptions. In the present case, we are trying to obtain a representation of the small-scale roughness of the core mantle boundary produced by the operation of the physically reasonable processes mentioned above. We use a cellular automata method as applied successfully in other fields in the last several decades [5]. Cellular automata consist of a discrete spatio-temporal dynamic system within a lattice of cells with a finite number of states. The discrete dynamic system is based on a set of rules, corresponding to an abstract representation of the microscopic-scale physics. It may lead to a wide range of macroscopic observables and a level of complexity unreachable with a classical continu-

ous approach [6]. Furthermore, these cellular automata techniques are efficient in the case of surface growth phenomena and reaction–diffusion processes [7]. Our cellular automaton has the following properties.

A vertical section of the CMB is modelled by a 2-D square lattice. The elementary cell has the characteristic dimension d of a crystal grain of the lower mantle rock, and L and H are respectively the length and the height of this regular lattice. At any time a cell can be in one of the following three states: [+]: crystal grain of the lower mantle rock, composed of oxygen and silicon; [0]: liquid iron alloy of the core, saturated in the light elements of the mantle; [−]: liquid iron alloy of the core, unsaturated in the light elements of the mantle.

The indices (i,j), $i\in[1,L]$, $j\in[1,H]$, label the Cartesian coordinates and the cell $c_{i,j}$ is either [+], [0] or [−] (Fig. 1a). We do not consider large-scale interaction like other discrete particle models [8], we only consider interactions between two neighboring cells with a common side (Von Neumann neighborhood, Fig. 1b). These doublets of neighboring cells are noted $(c_{i,j}, c_{i\pm1,j})$ and $(c_{i,j}, c_{i,j\pm1})$. This choice yields the lowest number of possible configurations and transitions (see Appendix and Tables 1 and 2) while allowing for complete modelling of all the physico–chemical processes that we consider (see Section 3).

The whole process is defined in terms of stationary transition rates between the various possible states of the doublets of neighboring cells. Recall that, given a transition rate λ_u^v from state u to v, the probability that a pair of neighboring cells in state u undergoes a transition towards the state v in the infinitesimal time interval dt is $\lambda_u^v dt$. We make a distinction between horizontal and vertical states: the gravity field imposes considering different transition rates for the doublets $(c_{i,j}, c_{i,j+1})$, $(c_{i,j}, c_{i,j-1})$, $(c_{i,j}, c_{i\pm1,j})$ (Fig. 1c).

As detailed below, a cell may change states only if it shares an edge with a neighboring cell in a different state. We choose periodic boundary conditions by respectively duplicating at every time step the state of the cells located at $i=1$, $i=L$, $j=1$, $j=H$ in the virtual cells located at $i=0$, $i=L+1$, $j=0$, $j=H+1$. The practical way we pro-
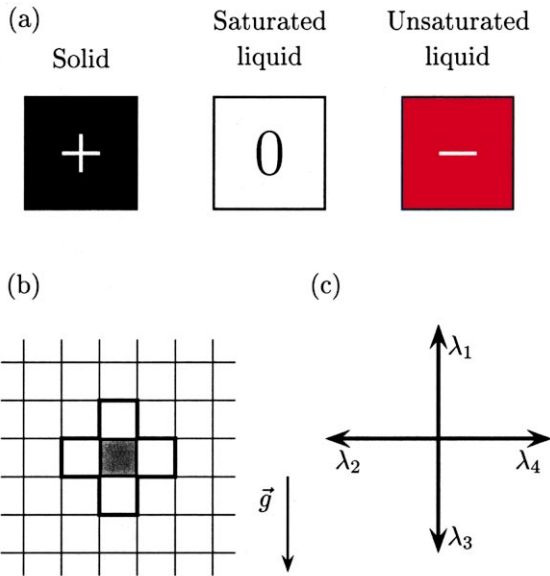
(a)

Solid | Saturated liquid | Unsaturated liquid

(b)   (c)

Fig. 1. (a) Different possible states of an elementary cell. (b) A part of the vertical section of the 2-D lattice. The shaded cell $c_{i,j}$ interacts only with his first neighbors $c_{i,j+1}$, $c_{i,j-1}$, $c_{i+1,j}$ and $c_{i-1,j}$ (bold line). (c) The transition rate λ depends on the orientation of the considered pair with respect to the gravity field $\vec{g}$. From symmetry considerations, we assume that $\lambda_2 = \lambda_4$.

ceed in the numerical simulations is detailed in the Appendix. The main point is that at each iteration three random numbers determine the time step, the doublet which undergoes a transition and the transition kind itself. This probabilistic approach and the physical processes represented by different set of transitions distinguish our model from classical deterministic cellular automata as Conway's game of life [9].

Each of the physico–chemical processes that we will now describe corresponds to a set of transitions. A transition of a given set cannot be considered in isolation because only combined and repeated actions are capable of reproducing these processes.

3. Physical processes

3.1. Dissolution

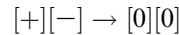We consider the dissolution of the grains of the

mantle into the unsaturated core fluid. This process depends on the grains being loosened by infiltration of the core fluid all around them, prior to dissolving in the unsaturated fluid. The characteristic time for infiltration around one grain τ_i is negligible compared with the time for dissolution of a grain τ_d.

Poirier and Le Mouël [4] have found that $\tau_i \approx 2.3 \times 10^6 d^2 \approx 250$ s, i.e., less than 5 min, for a grain size $d = 1$ cm [4]. The value of τ_d is given, following Berner [10] by:
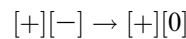
$$\tau_d = \frac{d^2 \rho_m}{2D\,(f_{sat} - f_0)\rho_c} \tag{1}$$

where $\rho_m \approx 5000$ kg m^{-3} is the density of the mantle material, $\rho_c \approx 10\,000$ kg m^{-3} is the density of the core fluid, D is the coefficient of diffusion of the light element in the core fluid, f_0 is the mass fraction of light elements in the fluid of the order of 10% and f_{sat}, the mass fraction at saturation. We can take $D \approx 3 \times 10^{-9}$ m^2 s^{-1} [4], but the value of f_{sat} is unknown; if we assume, for instance, that $f_{sat} = 2f_0$, we find that $\tau_d \approx 10^5$ s or about 28 h.

We assume that 1 cell of mantle saturates n cells of core fluid in light elements. The dissolution process involves two types of transition:
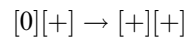
$$[+][-] \rightarrow [0][0]$$

with transition intensity λ_L.
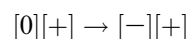
$$[+][-] \rightarrow [+][0]$$

with transition intensity $(n-2)\lambda_L$.

3.2. Crystallization

Mantle material is deposited from the saturated fluid, involving two types of transition (consistent with the condition that 1 cell of mantle saturates n cells of fluid):

$$[0][+] \rightarrow [+][+]$$

with transition intensity λ_C.

$$[0][+] \rightarrow [-][+]$$

with transition intensity $(n-1)\lambda_C$.

Thus, in average, n cells of saturated fluid deposit 1 cell of mantle (note that we talk here of the average on a great number of cells, as pointed out at the end of Section 2).

For the sake of simplicity, we make the assumption, compatible with dynamical equilibrium of the interface, that $\lambda_C = \lambda_L$. We may reasonably assume that λ_L is of the order of magnitude of $1/\tau_d$, i.e., $\lambda_C = \lambda_L \approx 10^{-5}$ s^{-1}. However, as τ_d depends on the value of $f_{sat} - f_0$, we may try several values.

Mass conservation during dissolution and crystallization is checked by computing at each time step the value of the following parameters:

$$S_{[+]}(t) = N_{[+]}(t) + \frac{1}{n}N_{[0]}(t) \tag{2}$$

and

$$S_{[-]}(t) = N_{[-]}(t) + \frac{n-1}{n}N_{[0]}(t) \tag{3}$$

where $N_{[+]}$, $N_{[0]}$ and $N_{[-]}$ are the number of [+], [0] and [−] cells, respectively. We verified that $S_{[+]}(t)$ and $S_{[-]}(t)$ remain constant.

3.3. Diffusion

We consider here the diffusion of light elements from cells of saturated fluid [0] into cells of unsaturated fluid [−]. For convenience purpose, we formally (and artificially) incorporate into the average diffusion process the effect of gravity, which makes the lighter saturated fluid float upward. We attribute the transition intensity λ_D, to diffusion in the horizontal direction:

$$[0][-] \rightarrow [-][0] \text{ and } [-][0] \rightarrow [0][-]$$

For diffusion in the upward vertical direction:

$$\begin{matrix} [-] \\ [0] \end{matrix} \rightarrow \begin{matrix} [0] \\ [-] \end{matrix}$$

we will take the transition intensity $\alpha\lambda_D$, with $\alpha > 1$.

For diffusion in the downward vertical direction:

$$\begin{matrix} [0] \\ [-] \end{matrix} \rightarrow \begin{matrix} [-] \\ [0] \end{matrix}$$

we will take the transition intensity $\beta\lambda_D$, with $\beta < 1$.

The numerical value of λ_D can be estimated by assuming that:

$$\lambda_D = \tau^{-1} = \frac{D}{d^2} \tag{4}$$

where τ is the characteristic time for diffusion and D the coefficient of diffusion of the light elements in the core fluid.

If we take $D \approx 3 \times 10^{-9}$ m^{2}s^{-1} [4], we find $\lambda_D \approx 3 \times 10^{-5}$ s^{-1} for $d = 1$ cm, of the same order of magnitude as λ_L, which is reasonable, as both constants are proportional to the characteristic time for diffusion.

The 20 possible transitions (10 horizontal and 10 vertical) with their intensities are shown in Tables 1 and 2 (Appendix).

Table 1
Transition intensities in the horizontal direction

λ_i^j	[+−]	[+0]	[−+]	[−0]	[0+]	[0−]
[++]	0	$\lambda_C = \lambda_L$	0	0	λ_C	0
[−−]	0	0	0	0	0	0
[00]	λ_L	0	λ_L	0	0	0
[+−]	0	$(n-1)\lambda_C$	0	0	0	0
[+0]	$(n-2)\lambda_L$	0	0	0	0	0
[−+]	0	0	0	0	$(n-1)\lambda_C$	0
[−0]	0	0	0	0	0	λ_D
[0+]	0	0	$(n-2)\lambda_L$	0	0	0
[0−]	0	0	0	λ_D	0	0

Table 2
Transition intensities in the vertical direction

λ_i^j	$\begin{bmatrix}+\\-\end{bmatrix}$	$\begin{bmatrix}+\\0\end{bmatrix}$	$\begin{bmatrix}-\\+\end{bmatrix}$	$\begin{bmatrix}-\\0\end{bmatrix}$	$\begin{bmatrix}0\\+\end{bmatrix}$	$\begin{bmatrix}0\\-\end{bmatrix}$
$\begin{bmatrix}+\\+\end{bmatrix}$	0	$\lambda_C = \lambda_L$	0	0	λ_C	0
$\begin{bmatrix}-\\-\end{bmatrix}$	0	0	0	0	0	0
$\begin{bmatrix}0\\0\end{bmatrix}$	λ_L	0	λ_L	0	0	0
$\begin{bmatrix}+\\-\end{bmatrix}$	0	$(n-1)\lambda_C$	0	0	0	0
$\begin{bmatrix}+\\0\end{bmatrix}$	$(n-2)\lambda_L$	0	0	0	0	0
$\begin{bmatrix}-\\+\end{bmatrix}$	0	0	0	0	$(n-1)\lambda_C$	0
$\begin{bmatrix}-\\0\end{bmatrix}$	0	0	0	0	0	$\beta\lambda_D$
$\begin{bmatrix}0\\+\end{bmatrix}$	0	0	$(n-2)\lambda_L$	0	0	0
$\begin{bmatrix}0\\-\end{bmatrix}$	0	0	0	$\alpha\lambda_D$	0	0

4. Realizations

4.1. Parameters

The parameters of the model are:

- The number n of cells of saturated fluid, which deposit 1 cell of mantle in average, is taken equal to 3.
- The size of an elementary cell, d, taken as the grain size of the mantle material. The value $d = 1$ cm, physically reasonable, has been adopted in the realizations.
- The diffusion coefficient D of the light element in liquid iron. The value $D \approx 3 \times 10^{-9}$ m^2 s^{-1} has been adopted here [4]. From this value and Eq. 4, we derive $\lambda_D \approx 3 \times 10^{-5}$ s^{-1} for $d = 1$ cm.

- The transition intensities for dissolution, crystallization and diffusion, λ_L, λ_C, λ_D, equal to the inverse of the characteristic times of the corresponding processes. The values of λ_L and λ_C, assumed to be equal, depend on D and on the difference $f_{sat} - f_0$ between the saturation concentration and the actual concentration of light elements in the core.

Three different realizations for different values of $f_{sat} - f_0$ are presented, with $f_{sat} = 2f_0$, $f_{sat} = 1.25f_0$, and $f_{sat} = 3f_0$, corresponding to $\lambda_C = \lambda_L \approx 10^{-5}$ s^{-1}, $\lambda_C = \lambda_L \approx 0.25 \times 10^{-5}$ s^{-1}, and $\lambda_C = \lambda_L \approx 2 \times 10^{-5}$ s^{-1} respectively.

- The coefficients α and β, embodying the effect of gravity on the vertical transition intensities. We have taken $\alpha = 1.05$ and $\beta = 1/1.05$

- The grid consists of 4000 columns and 500 rows of elementary cells (grains). It corresponds therefore to a section of CMB, 40 m long.

The simulations started from an initial state of the system consisting of mantle and core separated by a flat boundary. This is, of course, not considered as representing any physical reality, but it is convenient to monitor the appearance and evolution of small-scale roughness.
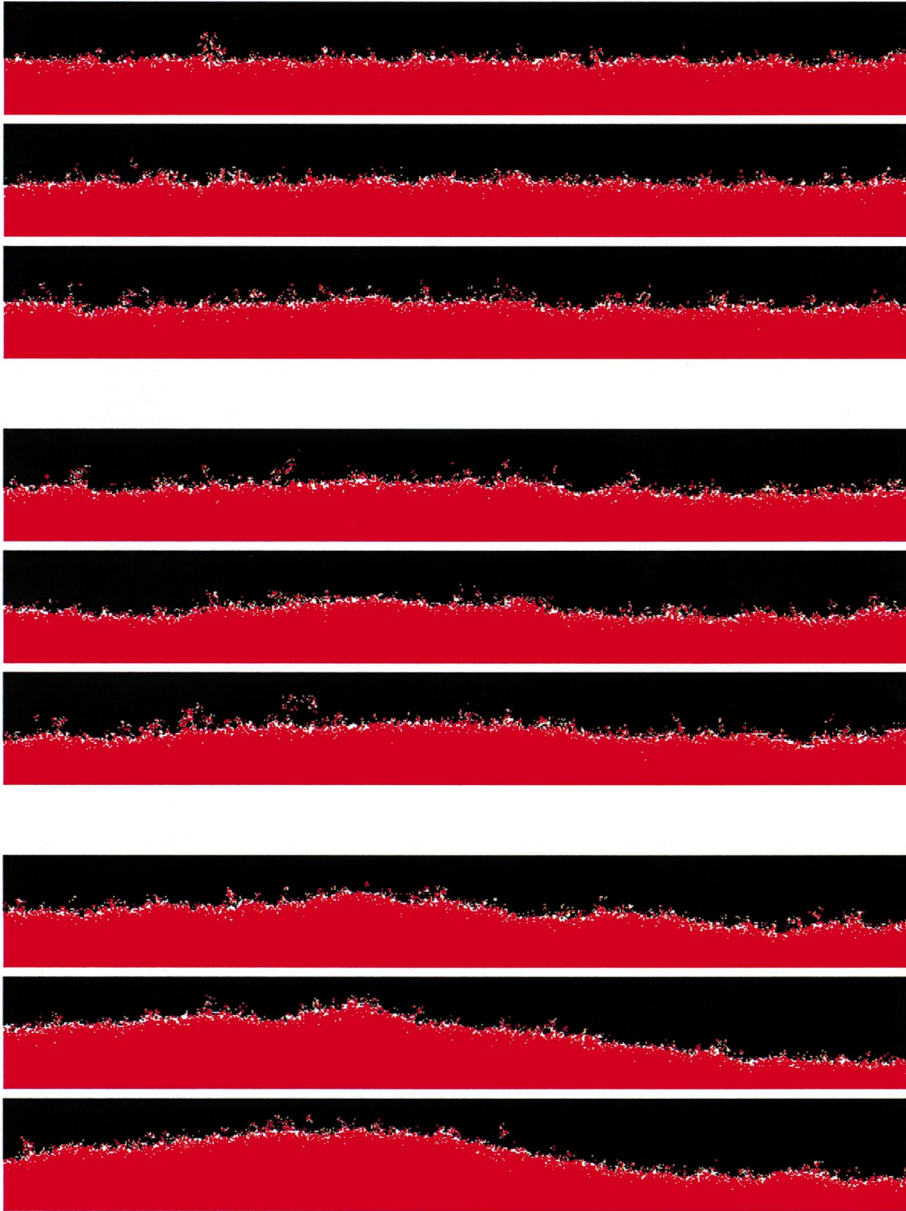

Fig. 2. Evolution with time of the small-scale core–mantle topography, starting from a flat CMB. $f_{sat} = 2f_0$; $\lambda_C = \lambda_L \approx 10^{-5}$ s^{-1}. The sections are 4000 cells long (40 m). Black: mantle; white: saturated liquid core; red: unsaturated liquid core. From top to bottom, we show the section after running the model computation for 10, 20, 40, 60, 80, 110, 300, 600 and 1000 years.

4.2. Results

In the first simulation $(\lambda_C = \lambda_L \approx 10^{-5}$ s$^{-1})$, 1.7×10^{11} transitions were effected. The times Δt between transitions were calculated from Eq. 19 (Appendix) and the total time corresponding to 1.7×10^{11} transitions is 3.17×10^{10} s, or about 1000 years. Fig. 2 shows the development of the small-scale topography of the boundary as a function of time. A blow-up of a short section of the boundary, about 1 m long, is shown in Fig. 3.

A boundary layer of saturated fluid soon appears at the interface; after 8×10^8 transitions (≈ 5 years), it is already well-established and its thickness (defined below) is statistically stationary, about 65 cm (Fig. 4, middle).

To characterize the boundary layer, we introduce the following variables:

- $h_s(i,t)$, depth of the first saturated liquid cell encountered from the top of the ith column of cells down, at time t.
- $h_l(i,t)$, depth of the last saturated liquid cell encountered from the top of the ith column of cells down, at time t.

The average thickness of the boundary layer is:

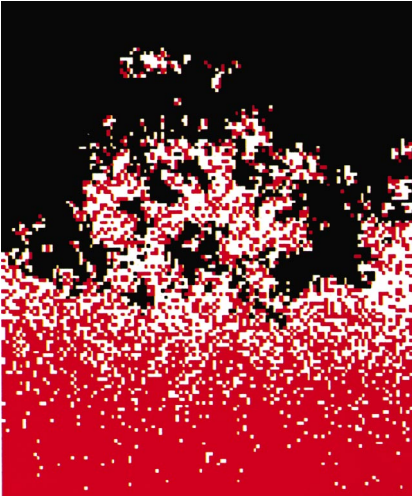$$\bar{h}(t) = \bar{h}_l(t) - \bar{h}_s(t) \tag{5}$$

Fig. 3. Blow-up of a short section (≈ 1 m long) of the boundary, after running the model computation for 110 years. A pixel corresponds to one cell, i.e., to one grain, 1 cm in size.
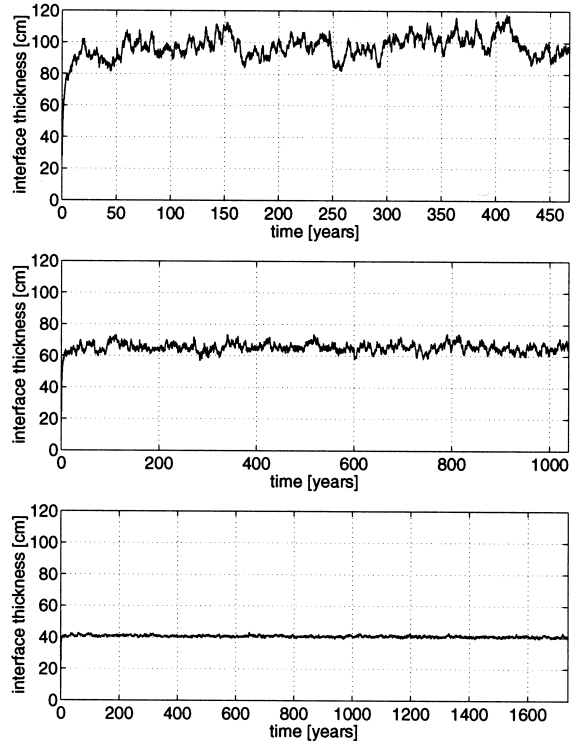

Fig. 4. Average thickness of the boundary layer, as a function of time. Top: $f_{sat} = 3f_0$; $\lambda_C = \lambda_L \approx 2 \times 10^{-5}$ s^{-1}; Middle: $f_{sat} = 2f_0$; $\lambda_C = \lambda_L \approx 10^{-5}$ s^{-1}; Bottom: $f_{sat} = 1.25f_0$; $\lambda_C = \lambda_L \approx 0.25 \times 10^{-5}$ s^{-1}. The time steps increase with $f_{sat} - f_0$, leading to different time in years for the same computation time, hence the different horizontal scales.

where $\bar{h}_s(t)$ is the average depth of the solid–liquid interface, i.e., the average of $h_s(i,t)$ over the L columns along the length of the grid,

$$\bar{h}_s(i,t) = \frac{1}{L}\sum_{i=1}^{L} h_s(i,t) \tag{6}$$

and $\bar{h}_l(t)$ is the average depth of the saturated liquid-unsaturated liquid interface, i.e., the average of $h_l(i,t)$ over the L columns along the length of the grid.

$$\bar{h}_l(i,t) = \frac{1}{L}\sum_{i=1}^{L} h_l(i,t) \tag{7}$$

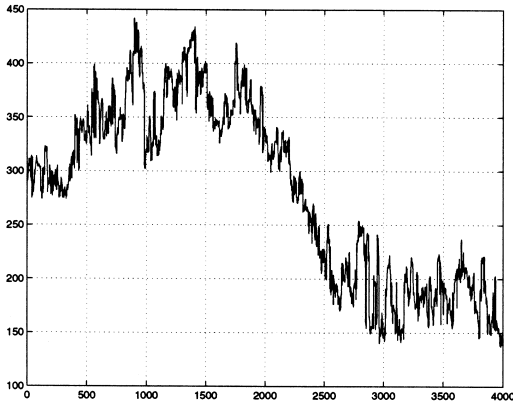The profile h_s of the upper interface, over the whole length, at the end of the simulation, is shown in Fig. 5.

Fig. 5. Profile of the upper interface (mantle-saturated core) for $f_{sat} = 2\ f_0$; $\lambda_C = \lambda_L \approx 10^{-5}$ s^{-1} after running the model computation for 1000 years. The vertical scale is exaggerated (initial planar interface at 250 cm).

The solid–liquid interface (upper interface) and the saturated–unsaturated fluid interface (lower interface), are characterized by their roughnesses $R_u(t)$ and $R_l(t)$ respectively, defined by:

$$R_u(t) = \sqrt{\frac{1}{L}\sum_{i=1}^{L}[h_s(i,t) - \bar{h}_s(i,t)]^2} \qquad (8)$$

and:

$$R_u(t) = \sqrt{\frac{1}{L}\sum_{i=1}^{L}[h_s(i,t) - \bar{h}_s(i,t)]^2} \qquad (9)$$

The upper and lower roughnesses are shown, as a function of time, in Figs. 6 and 7, middle. After about 600 years, they reach a statistical steady state, on which oscillations in time are superimposed.

The power spectrum of the upper profile (Fig. 5) is shown in Fig. 8. It is a spectrum in $f^{-1.5}$. After about 10^{10} transitions (about 50 years), an undulation of the boundary appears, with an apparent dominant wavelength of the order of a few tens of meters (Fig. 2).

Not surprisingly, the amplitude of the oscillations in time of the roughness of the upper interface between solid mantle and liquid saturated core is greater than that of the oscillations of the lower interface between liquid saturated and unsaturated core.

The distance from saturation of the core $f_{sat} - f_0$ plays a great role in the evolution of the calculated profile of the CMB.

When the actual concentration f_0 is chosen farther from the saturation concentration in light elements f_{sat} ($f_{sat} = 3f_0$; $\lambda_C = \lambda_L \approx 2 \times 10^{-5}$ s^{-1}), the kinetics of dissolution and crystallization are faster, the thickness of the boundary layer increases up to about 90 cm and its oscillations in time are more pronounced (Fig. 4, top). The roughnesses of the upper and lower boundaries behave in a similar fashion: they are greater than for $f_{sat} = 2f_0$; $\lambda_C = \lambda_L \approx 10^{-5}$ s^{-1}, and their oscillations are more marked (Figs. 6 and 7, top). Conversely, closer to the saturation concen-
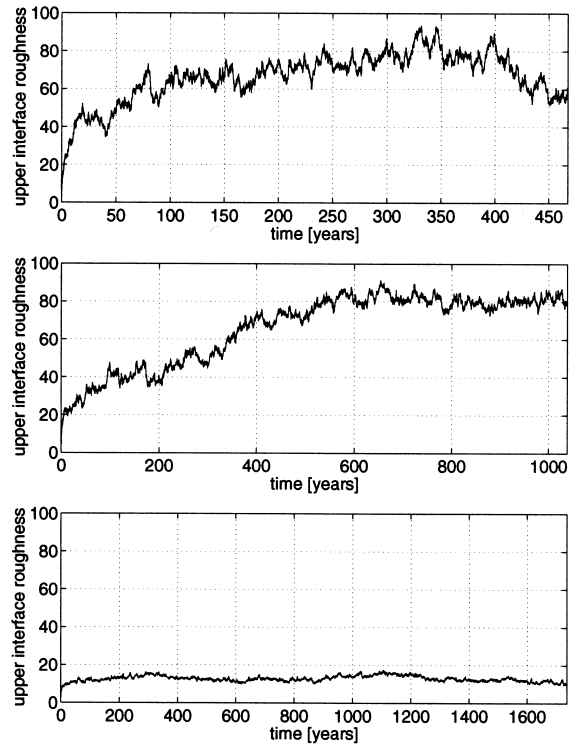

Fig. 6. Roughness of the upper interface (mantle-saturated core) as a function of time. Top: $f_{sat} = 3f_0$; $\lambda_C = \lambda_L \approx 2 \times 10^{-5}$ s^{-1}; middle: $f_{sat} = 2f_0$; $\lambda_C = \lambda_L \approx 10^{-5}$ s^{-1}; bottom: $f_{sat} = 1.25f_0$; $\lambda_C = \lambda_L \approx 0.25 \times 10^{-5}$ s^{-1}. The time steps increase with $f_{sat} - f_0$, leading to different time in years for the same computation time, hence the different horizontal scales.

tration $(f_{sat} = 1.25 f_0; \quad \lambda_C = \lambda_L \approx 0.25 \times 10^{-5} \text{ s}^{-1})$ the boundary layer is thinner, about 40 cm, and practically does not oscillate in time (Fig. 4, bottom). The roughnesses also have smaller values, more stable in time (Figs. 6 and 7, bottom).

5. Conclusions

It is natural to consider that the CMB is not a smooth spheroïdal surface and that it exhibits irregularities on various scales. Long wavelength topography is investigated by seismological methods [11,12]. In the present work, we have attempted to model and describe the very small-scale roughness of the CMB, based on the con-
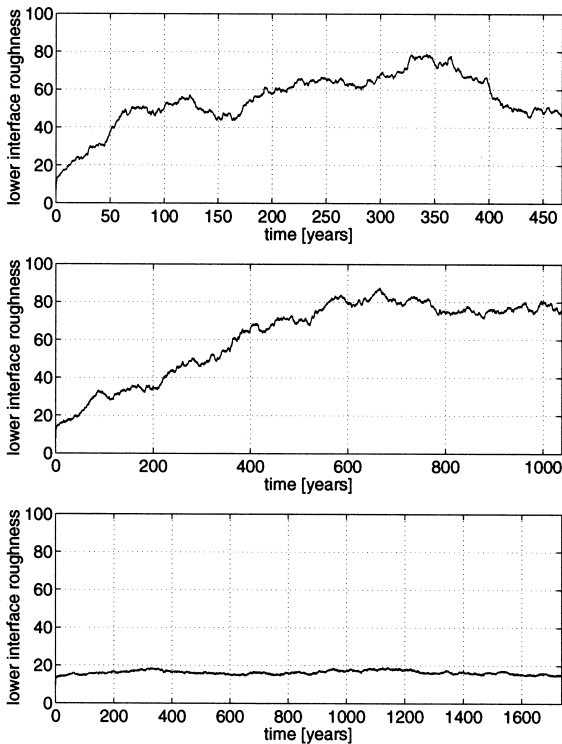

Fig. 8. Power spectrum of the upper boundary profile for $f_{sat} = 2\, f_0;\ \lambda_C = \lambda_L \approx 10^{-5} \text{ s}^{-1}$ after running the model computation for 1000 years.

Fig. 7. Roughness of the lower interface (saturated–unsaturated core) as a function of time. Top: $f_{sat} = 3 f_0$; $\lambda_C = \lambda_L \approx 2 \times 10^{-5} \text{ s}^{-1}$; middle: $f_{sat} = 2 f_0$; $\lambda_C = \lambda_L \approx 10^{-5} \text{ s}^{-1}$; bottom: $f_{sat} = 1.25 f_0$; $\lambda_C = \lambda_L \approx 0.25 \times 10^{-5} \text{ s}^{-1}$. The time steps increase with $f_{sat} - f_0$, leading to different time in years for the same computation time, hence the different horizontal scales.
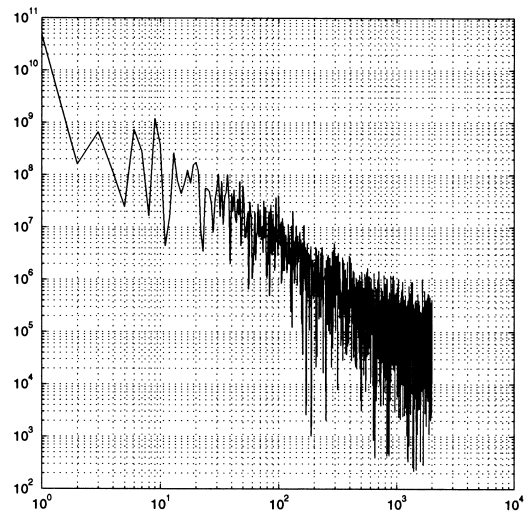
sideration of physical mechanisms. There is, however, a question we cannot escape. We have performed a 2-D computation, whereas we should have computed a topography over the CMB, a curved surface in 3-D space. As it is generally the case, it is not easy to prove a priori that a 3-D computation would give results qualitatively similar to the 2-D one. Nevertheless, referring to more or less analog situations [7], we think the results are not likely to be very different in the present case. At any rate, a 3-D code is planned.

The model predicts that the CMB could exhibit a small-scale topography h_s of the order of tens of centimeters, which it is interesting to compare with the thickness of the thermal boundary layer δ_{th} and of the Ekman layer δ_E. To this end, we use straightforward classical formulas, valid in systems with much simpler geometries, without expecting more than orders of magnitude.

The thickness δ_{th} of the thermal boundary layer is calculated, from the boundary layer theory, as a function of the Rayleigh number Ra [13]:

$$\delta_{th} \approx 1.7\, h \text{Ra}^{-\frac{1}{3}} \tag{10}$$

where h is the height of the convecting cell. Taking reasonable values of the outer core parameters entering the Rayleigh number [14], i.e., thermal

expansion coefficient, thermal diffusivity, kinematic viscosity, height and temperature difference between top and bottom, respectively equal to: $\alpha \approx 6 \times 10^{-6}$ K^{-1}, $\kappa \approx 10^{-5}$ m^2 s^{-1}, $\nu \approx 10^{-7}$ m^2 s^{-1}, $h \approx 2 \times 10^6$ m, $\Delta T \approx 2000$ K, we find Ra $\approx 10^{30}$ and $\delta_{\text{th}} \approx 5 \times 10^{-4}$ m, i.e., a thickness of the thermal boundary layer of about 1 mm.

The thickness of the viscous Ekman layer of the fluid flow in the core is given by [15]:

$$\Delta \approx \sqrt{\frac{\nu}{\Omega}} \tag{11}$$

where ν is the kinematic viscosity of the core fluid and Ω is the angular velocity of the Earth. We find $\Delta \approx 3 \times 10^{-2}$ m, or about 3 cm.

We are aware of the problematic validity of the formulas used, in the case of boundary layers close to an interface with a roughness such as the one illustrated in Fig. 3. However, it seems reasonable to conclude that our model predicts that the roughness of the CMB should extend into the core over a distance larger than the thickness of the thermal boundary layer and the Ekman layer. If this is indeed the case in reality, one could expect the fluid flow in the core to interact with the small-scale roughness of the CMB [16] and lead to some sort of dissipation, of a nature so far not investigated.

Acknowledgements

Appendix

The dynamical process of evolution is defined as a stationary stochastic process. Transitions from one state to another and the evolution of the system from time t to time $t+\Delta t$ are then only determined from the knowledge of the state of the system at time t. A cell can change states only if it shares an edge with a neighboring cell in a different state. We therefore consider doublets. In this three states model ([+], [0] and [−]) with only first neighborhood interactions, the different doublets ($c_{i,j}$, $c_{i,j+1}$) and ($c_{i,j}$, $c_{i+1,j}$) are [+][+], [+][0], [+][−], [0][+], [0][0], [0][−], [−][+], [−][0] and [−][−].

The total number of different horizontal and vertical doublets is therefore: $N_D = 18$

The doublets composed of cells in the same state ([+][+], [0][0], [−][−]) cannot change states, hence the total number of doublets that can change states is: $N_t = 12$

The grid consists of $L \times H$ cells. As the cells at opposite edges cannot form doublets, the total number of doublets in the grid is:

$$N = H(L-1) + L(H-1) \tag{12}$$

The number of doublets in the state i ($1 \leq i \leq N_D$) is N_i, with:

$$N = \sum_{i=1}^{N_D} N_i \tag{13}$$

There are 20 possible $i \rightarrow j$ transitions (see Section 3 and Tables 1 and 2).

The transition intensity per unit time (with the dimension of frequency) of each doublet, from state i to state j ($1 \leq j \leq N_D$) is λ_i^j and the total transition intensity for each doublet in state i is:

$$\lambda_i = \sum_{j=1}^{N_D} \lambda_i^j \tag{14}$$

The transition intensity for any doublet in state i to go to state j is:

$$\pi_i^j = N_i \lambda_i^j \tag{15}$$

The total transition intensity of the system is:

$$\pi = \sum_{i=1}^{N_D} N_i \lambda_i = \sum_{i=1}^{N_D} \sum_{j=1}^{N_D} N_i \lambda_i^j \tag{16}$$

The statistical weight of each transition is:

$$P_i^j = \frac{\pi_i^j}{\pi} \tag{17}$$

Eqs. (12–17) govern the evolution of the system and only depend on the state at time t. As said above it is a process without memory.

At the time t of the last transition, we must choose the time $t+\Delta t$ at which a new transition will occur in the system. We assume that the probability of a transition in the system after Δt is given by the function $F(\Delta t)$, such that $0 < F(\Delta t) < 1$:

$$F(\Delta t) = 1 - e^{-\pi \Delta t} \tag{18}$$

where π, known at time t, is given by Eq. 16. A value R_t of $F(\Delta t)$ is drawn at random ($0 \leq R_t \leq 1$) and the corresponding value of Δt is (Fig. 9):

$$\Delta t = -\frac{1}{\pi} \ln(1 - R_t) \tag{19}$$

To determine which transition $i \rightarrow j$ is occurring in the system at $t+\Delta t$, we first label the possible $i \rightarrow j$ transitions with an index k ($1 \leq k \leq 20$, see Section 3 and Tables 1 and 2) and we construct a cumulative function CF_k, such that:
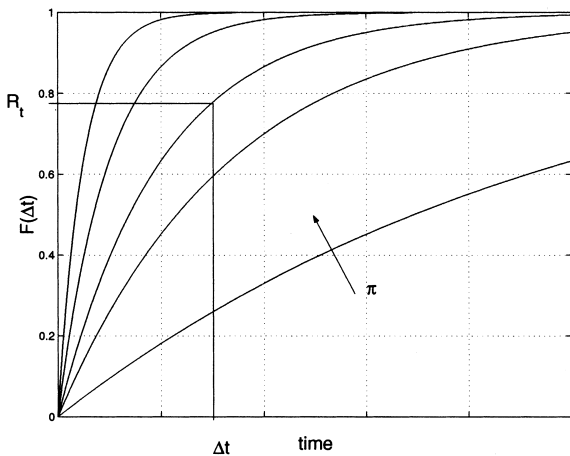
$$CF_k = \pi_k + CF_{k-1} \tag{20}$$

Fig. 9. Determination of the time interval Δt between two successive transitions. A value R_t of $F(\Delta t)$ is drawn at random and $\Delta t = -(1/\pi)\ln(1-R_t)$. The arrow indicates the direction of increasing values of π.

where $\pi_k \equiv \pi_i^j = N_i \lambda_i^j$ for the kth transition, and $\pi_1 \leq CF_k \leq \Sigma \pi_k$. We then draw at random a value R_c ($0 < R_c \leq 1$). The chosen transition k is the transition such that $CF_{k+1} \geq R_c \pi$. This procedure ensures that transitions with a high probability are drawn more often than those with a low probability.

As the doublets of the system in state i are numbered, we finally determine which doublet has been affected by the transition by drawing a number R_w at random ($0 \leq R_w \leq N_i$).

We then have a new system at $t+\Delta t$, on which we can repeat the same operations: calculation of N and choice of transition and of the transiting doublet. The evolution of the system is given by many iterations; it is governed by the values of the transition intensities, depending on the physical nature of the processes taking place at the CMB.

Although the physical mechanisms occur on the atomic scale, we consider the processes taking place on the scale of the grain. Furthermore, it must be kept in mind that the processes described here represent an average on a great number of cells and are meaningless on the scale of one doublet.

References

[1] J.P. Poirier, Transport properties of liquid metals and viscosity of the Earth's core, Geophys. J. 92 (1988) 99–105.

[2] J.L. Le Mouël, G. Hulot, J.P. Poirier, in: D.J. Crossley (Ed.), Core–mantle interactions, Earth's Deep Interior, Gordon and Breach, London, 1997, pp. 197–221.

[3] E. Knittle, R. Jeanloz, Simulating the core–mantle boundary: An experimental study of high-pressure reactions between silicate and liquid iron, Geophys. Res. Lett. 16 (1989) 609–612.

[4] J.P. Poirier, J.L. Le Mouël, Does infiltration of core material into the lower mantle affect the observed geomagnetic field?, Phys. Earth Planet. Inter. 73 (1992) 29–37.

[5] B. Chopard, M. Droz, Cellular Automata Modeling of Physical Systems, Cambridge University Press, Cambridge, 1998.

[6] D. Rothman, S. Zaleski, Lattice-Gas Cellular Automata: Simple Models of Complex Hydrodynamics, Collection Aléa. Cambridge University Press, Cambridge, 1997.

[7] A. Barabási, E. Stanley, Fractal Concepts in Surface Growth, Cambridge University Press, Cambridge, 1995.

[8] W. Dzwinel, D.A. Yuen, A two-level, discrete particle approach for large scale simulation of colloidal aggregates, Int. J. Mod. Phys. C 11 (2000) 1037–1061.

[9] M. Gardner, The fantastic combinations of John Conway's new solitaire game life, Sci. Am. 220 (1970) 120.

[10] R.A. Berner, Rate control of mineral dissolution under Earth surface conditions, Am. J. Sci. 278 (1978) 1235–1252.

[11] E.J. Garnero, Heterogeneity of the lowermost mantle, Annu. Rev. Earth Planet. Sci. 28 (2000) 509–537.

[12] D.J. Doornbos, T. Hilton, Models of the core–mantle boundary and the travel time of reflected core phases, J. Geophys. Res. 94 (1989) 15741–15751.

[13] D.L. Turcotte, G. Schubert, Geodynamics, Wiley, New York, 1982.

[14] J.P. Poirier, Physical properties of the Earth's core, C. R. Acad. Sci. Paris 318 (II) (1994) 341–350.

[15] D.J. Tritton, Physical fluid dynamics, Van Nostrand Reinhold, New York, 1977.

[16] Y.B. Du, P. Tong, Enhanced heat transport in turbulent convection over a rough surface, Phys. Rev. Lett. 81 (1998) 987–990.